Study of the Conductive Properties of Two-Component Xerographic Developer Materials*

E. J. Gutman† and G. C. Hartmann†

Joseph C. Wilson Center for Technology, Xerox Corporation, Webster, New York 14580

This study is an investigation of the electrical conductivity of two-component developer materials using a measurement cell that reproduces the electric, magnetic, and geometric characteristics of the xerographic development zone. Measurements were made on model developer materials having a range of properties. The measured current depends on whether the developer roll is at rest or rotating. For the static case, the dependencies of two-component developer conductivity on electric field, toner concentration, toner and carrier size, and carrier surface roughness were measured. A physical model is proposed, compared to the measurements, and shown to describe the major observations. For the dynamic case in which the roller is turning during the measurement, there are additional current contributions due to contact charging of the developer with the electrodes and displacement currents due to motion of charged toner and carrier particles. A physical model for the voltage dependence is proposed and used to separate the currents.

Journal of Imaging Science and Technology 40: 334–346 (1996)

Introduction

The electrical conductivity of two-component developers is an important parameter that affects the solid area, line, and halftone development efficiency and background development in xerography. Experiments with insulating developer materials show strong line edge development, associated with electrostatic fringe fields, but poor fill-in of large uniform solid areas. In contrast, experiments with conductive developer materials show that fringe field development is suppressed and solid area development is more uniform. These characteristics have been investigated for two-component development in earlier work.[1–3] Hays[2] has considered the flow of charge through a conductive developer and the dependence on electric field, magnetic field, toner concentration, and developer agitation. Hoshino[4] has also investigated the dependence of developer conductivity on electric and magnetic fields. He pointed out that the current increases more rapidly than linearly with the electric field, and he suggested that conduction is limited by the oxide layer on the surface of the metal carrier beads. Nash and Bickmore[5] have discussed the aging process for conductive developers. They found that both the carrier conductivity and the coefficient for the dependence of developer conductivity on toner concentration, α, change over time with developer usage. They identified carrier abrasion and toner impaction as the key underlying physical mechanisms responsible for these changes.

This study presents an investigation of the electrical conductivity of two-component developer materials using a measurement cell with a development roll that reproduces the electric, magnetic, and geometric characteristics of the xerographic development zone. Developer conductivity depends on several externally controllable parameters, such as applied voltage, magnetic field, developer roll speed, and toner concentration, as well as on material design parameters, such as toner and carrier size, composition, and shape. Consequently, to understand the underlying physical mechanisms, a systematic investigation is needed in which the individual phenomena are separately modeled. The first part of the study investigates static mode measurements when the developer roll is at rest. This part is subdivided into an investigation of carrier beads without toner particles and an investigation of developers with varying concentrations of toner. The second part of the study examines dynamic mode measurements when the developer roll is turning. Although dynamic mode measurements are considered, our emphasis is on the static mode measurements. A final section summarizes our findings.

The geometry of the carrier and toner particles in the zone between the measurement electrode and the roller is complicated. The carrier typically has a metal core surrounded by an oxide layer, which in turn may be partially covered by an insulating layer of polymer. The toner particles break the electrical contacts between beads. When a voltage is applied between the roller and the electrode, the voltage drop is across the oxide layers and toner particles, because the metal cores act as electrical short circuits. The toner particles are much more insulating than the oxide layers, so the current will flow only through the metal cores and oxide layers, and the magnitude will be controlled by the oxide layers. Consequently, the system can be represented by a simplified geometry of two metal electrodes and an oxide film that simulates the cumulative effect of all the contacting oxide surfaces of the carrier beads.

Metal–oxide conduction[6] can be described by a Schottky model if the conduction is limited by the metal–oxide interfacial barrier,

$$J = J_0 \exp\left(\frac{\beta_s E^{0.5}}{kT}\right),$$

where $\beta_s = (e^3/4\pi\varepsilon)^{0.5}$; or by the Poole–Frenkel model if the conduction is limited by the bulk oxide,

Original manuscript received December 22, 1995. Revised May 3, 1996.

* Presented in part at IS&T 's 11th International Congress on Advances in Non-Impact Printing Technologies, October 29 – November 3, 1995, Hilton Head, SC.

† IS&T Member

$$J = J_0 \exp\left(\frac{\beta_{pf} E^{0.5}}{2kT}\right),$$

where $\beta_{pf} = (e^3/\pi\varepsilon)^{0.5}$. In the case of the Schottky model,[6] the prefactor J_0 is independent of the applied electric field E if the electron mean free path λ is greater than the oxide layer thickness, and J_0 is equal to $(\sigma_0 E)$ if λ is much less than the oxide layer thickness. For our situation, we believe that λ is small compared with the oxide layer thickness; consequently, for a single oxide layer, both models lead to a current density of the form:

$$J = J_0 \exp\left(\frac{(e^3 E / \pi\varepsilon)^{0.5}}{2kT}\right), \quad (1)$$

where J_0 is the low field current density given by $\sigma_0 E$, E is the applied electric field, σ_0 is the ohmic conductivity, e is the electronic charge, ε is the dielectric permittivity, k is Boltzmann's constant, and T is the absolute temperature.

The relation between the current through a single oxide layer, Eq. 1, and a bed of developer consisting of many carrier beads is a complex problem that we do not address explicitly. However, the electric field dependence is expected to be similar to Eq. 1. Consequently, we assume the following dependence of current on applied voltage,

$$I = G_0 V \exp(BV^{0.5}) = G_V V, \quad (2)$$

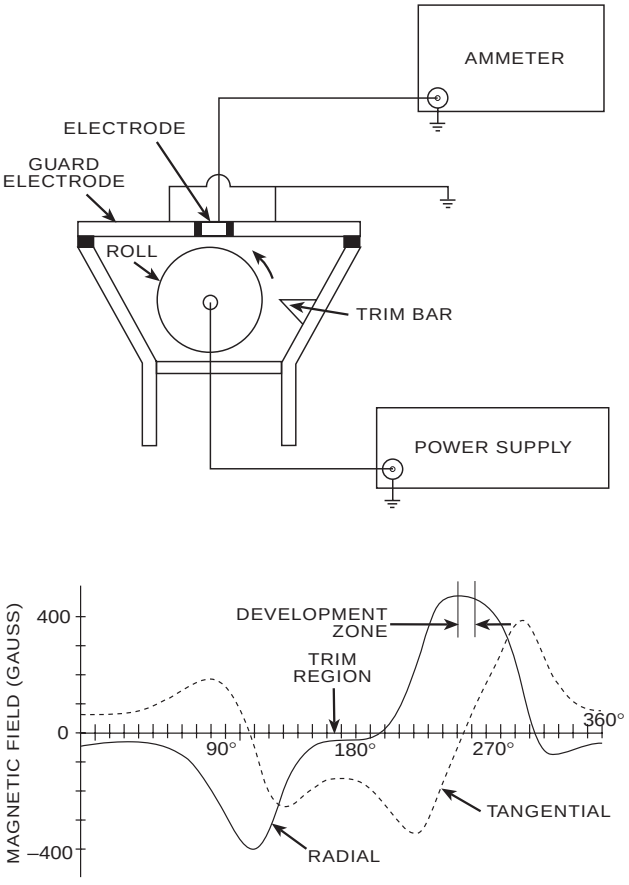

Figure 1. Diagram of the experimental measurement cell. The cylinder can be rotated. Inside the cylinder are two stationary magnets. The radial and tangential magnetic fields generated by the magnets are also shown.

where G_0 is the Ohmic conductance, V is the applied voltage, and B is the Poole–Frenkel related parameter $(e^3/\pi\varepsilon l)^{0.5}/2kT$. We interpret l as the effective thickness of the oxide film that simulates the cumulative effect of all the oxide surfaces on the carrier beads. Because all measurements in this study were made at room temperature, we have incorporated kT into the parameter B.

Measurement Procedure

We used the miniature magnetic brush cell illustrated in Fig. 1. The cell includes a magnetic brush roll, made with a 3.8 cm diameter by 9.5 cm long nonmagnetic steel cylinder with a surface of approximately 13 μm roughness, which helps transport the developer material. The cylinder is rotated by a motor at a surface speed of 25 cm/s. Inside the cylinder, there is a stationary permanent magnet assembly whose shape was designed to give the magnetic field profile shown in Fig. 1. This profile approximates the magnetic fields used in xerographic development. A trim bar with an adjustable gap is located at the three o'clock position, where the tangential magnetic field is strong. The cell holds about 50 cc of carrier or developer material. The top of the cell is a segmented flat plate with a rectangular measurement electrode surrounded by a guard electrode. The rectangular electrode is 0.5 cm wide by 6 cm long. It is located in the constant radial magnetic field of the development zone. The current was measured using the ammeter mode of a Keithley 610C electrometer.

The measurement procedure is described next. First, both the trim bar gap and the cylinder-to-electrode gap were set to 2.54 mm. Approximately 50 cc of developer or carrier material was put into the cell, and the steel cylinder was rotated for 3 min. Two measurement modes were used: static and dynamic. For the static measurement, the cylinder was stopped, the voltage was applied, and a current reading was made 15 s later. To measure the I–V characteristic, this process was repeated with voltages stepped in equally spaced $\sqrt{V}$ increments. The voltage was increased until breakdown occurred or until 1000 V was reached. In some cases, the current for a fixed voltage was measured, and we calculated the developer conductivity, using the expression

$$\sigma_V = \frac{l_s}{A}\frac{I}{V} = \frac{l_s}{A} G_V,$$

where l_s is the cylinder-to-electrode spacing, A is the area of the electrode, and I/V is related to G_V by Eq. 2. A positive voltage was usually applied to the cylinder. Measurements were also made with negative voltages; within the precision of the measurements, in the static mode the polarity did not affect the magnitude of the current.

For the dynamic measurement, the voltage was applied and the current was measured while the cylinder was rotated. Two instruments were used to measure the dynamic current, i.e., the ammeter mode of the Keithley 610C electrometer or an *xy* plotter connected across a small precision resistor. With the *xy* plotter, the current was recorded as a function of the applied voltage, which was increased linearly in time. To measure the I–V characteristic, the voltage was stepped, following a procedure similar to the static mode of measurement. The dynamic mode conductivity was defined as the slope of the I–V data at 0 V. The *xy* plotter method facilitated this measurement.

Preliminary measurements indicated that the conductivity depended on the angular position of the magnet assembly with respect to the top plate. This effect was investigated to select a standard angular position for the magnet assembly and a standard width for the measure-

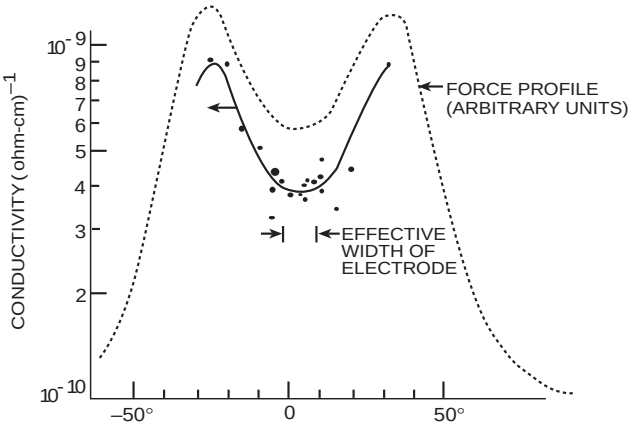

Figure 2. Measurements of the conductivity as a function of the angular position of the magnet assembly. The calculated strength of the magnetic force is shown for comparison. There is good correspondence between the measured conductivity and the calculated magnetic force.

ment electrode. The angular position of the magnet assembly was defined by the angle between the line normal to the electrode surface and the line normal to the development magnet. The magnet assembly was positioned at various angles over a range of ±30°. For each position, the static mode conductivity was measured as shown in Fig. 2. The conductivity varies smoothly with magnet angle and exhibits a broad minimum centered at 0°. The electrode width was selected to match the region where the conductivity was approximately constant. With this choice, the variation in conductivity would be small if the angular position of the magnet were in error by a few degrees.

We will briefly discuss the physical mechanism for the dependence of conductivity on the angular position of the magnet assembly. The key variable is the magnetic force, which compresses the developer material and improves the contacts between carrier beads. For carrier beads in a uniform magnetic field, Hoshino[4] showed that the conductivity increased with the strength of the magnetic field. In our case, the magnetic field and the associated magnetic force vary with the angular position of the magnet assembly. To examine the effect more directly, the magnetic force was calculated from the magnetic field measurements shown in Fig. 1. We show in Fig. 2 that over the small range of magnetic force generated by our magnet assembly, the conductivity correlates with the strength of the magnetic force.

Investigation of Static Mode Conductivity

Carrier Beads. Many model carrier materials were prepared and measured. For this section, four carrier bead samples with different size, shape, and surface roughness were selected. Scanning electron micrographs of these carrier beads are shown in Fig. 3. The surface oxidation of the samples was monitored by the color, which varied from silver to blue. The rough-round and the smooth-grit carriers had a bluish color, indicating either more oxide or a different species of oxide than was indicated by the silvery gray color of the other two carriers. Figure 4 shows the current–voltage data measured in the static mode for four carrier samples with different morphologies, particularly surface roughness and shape.

A nonlinear least-squares method was used to determine the two parameters G_0 and B in Eq. 2, as shown in Table I. We found that the I–V data can be accurately represented by Eq. 2. Data for other carrier bead samples with similar morphology but from different lots can also be represented by Eq. 2, but the values of G_0 and B vary somewhat. Experiments were done to check that this variability was not caused by the measurement procedure. We attribute this variability to variations in the amount and type of oxide on the carrier surface, which was not characterized. The experiments reported in this study were designed so that these variations did not influence our interpretation of the data.

TABLE I. Values of G_0 and B for Four Types of Carrier Beads

Morphology	Smooth-round	Rough-round	Smooth-grit	Rough-grit
G_0 (Ω^{-1})	1.2×10^{-7}	7.0×10^{-6}	1.3×10^{-9}	3.8×10^{-6}
B ($V^{-0.5}$)	0.78	0.46	0.83	0.78

There is no obvious relationship between the morphology and the values of G_0 and B; evidently these values depend on the surface oxidation, although additional experiments are required to determine the detailed dependence. The value of B ranges from 0.5 to 0.8 $V^{-0.5}$. The effective oxide layer thicknesses calculated from these values are 0.25 to 0.6 μm, using a value of 14 for the dielectric constant of ferrous oxide.[7] The thickness of the oxide layer on the surface of the carrier bead sample inferred from measurements of the weight fraction of oxygen, about 10^{-3}, is 0.1 μm. Although this is the same order of magnitude as the effective oxide thickness deduced from conductivity measurements, a careful comparison requires a model of the developer using a parallel and series resistor network, which is beyond the scope of this study.

From Fig. 4, we conclude that the shape of the current–voltage curve can be accurately represented by an equation of the form of Eq. 2 with appropriately chosen values of the parameters G_0 and B.

Developers. The current–voltage characteristic is modified if toner is mixed with carrier beads. A developer was prepared by mixing toner and carrier. The toner concentration of the developer was reduced with a three-step procedure. First, the developer was split into two portions. Second, toner was removed from one portion. Finally, the carrier recovered from this portion was blended back into the other portion and mixed.

The I–V curves were measured for developers made using rough-grit carrier beads of about 100 μm diameter, which had a small amount of polymer coating to control the triboelectric charge. The small amount of polymer coating had no appreciable effect on the I–V curves. A commercial toner with a number median diameter of 9 to 10 μm was used. The I–V measurements made on these developers are shown in Fig. 5. The data set for each toner concentration was fit to Eq. 2. The results, which are displayed in Fig. 6, show that the parameter B is independent of toner concentration. However, the Ohmic conductance parameter, G_0, decreases rapidly as toner concentration is increased. Hoshino[4] obtained similar results. Recognizing that B is independent of toner concentration, another fit was calculated using all the data, but with a single value of B and separate values of G_0. This result is shown by the lines in Fig. 5. Table II lists the values of G_0 and B for the separate data sets, as well as the G_0 values for the second fit with a common value of B. The differences between the two sets of G_0 values are not significant. The G_0 data in Table II and Fig. 6 can be represented approximately by an empirical relationship of the form:

$$G_0(C) = G_0(0)\exp(-\alpha C), \tag{3}$$

where C is toner concentration, $G_0(0)$ is the ohmic conductance when C equals 0, and α is a parameter that characterizes the semilogarithmic slope. The value of α from a fit

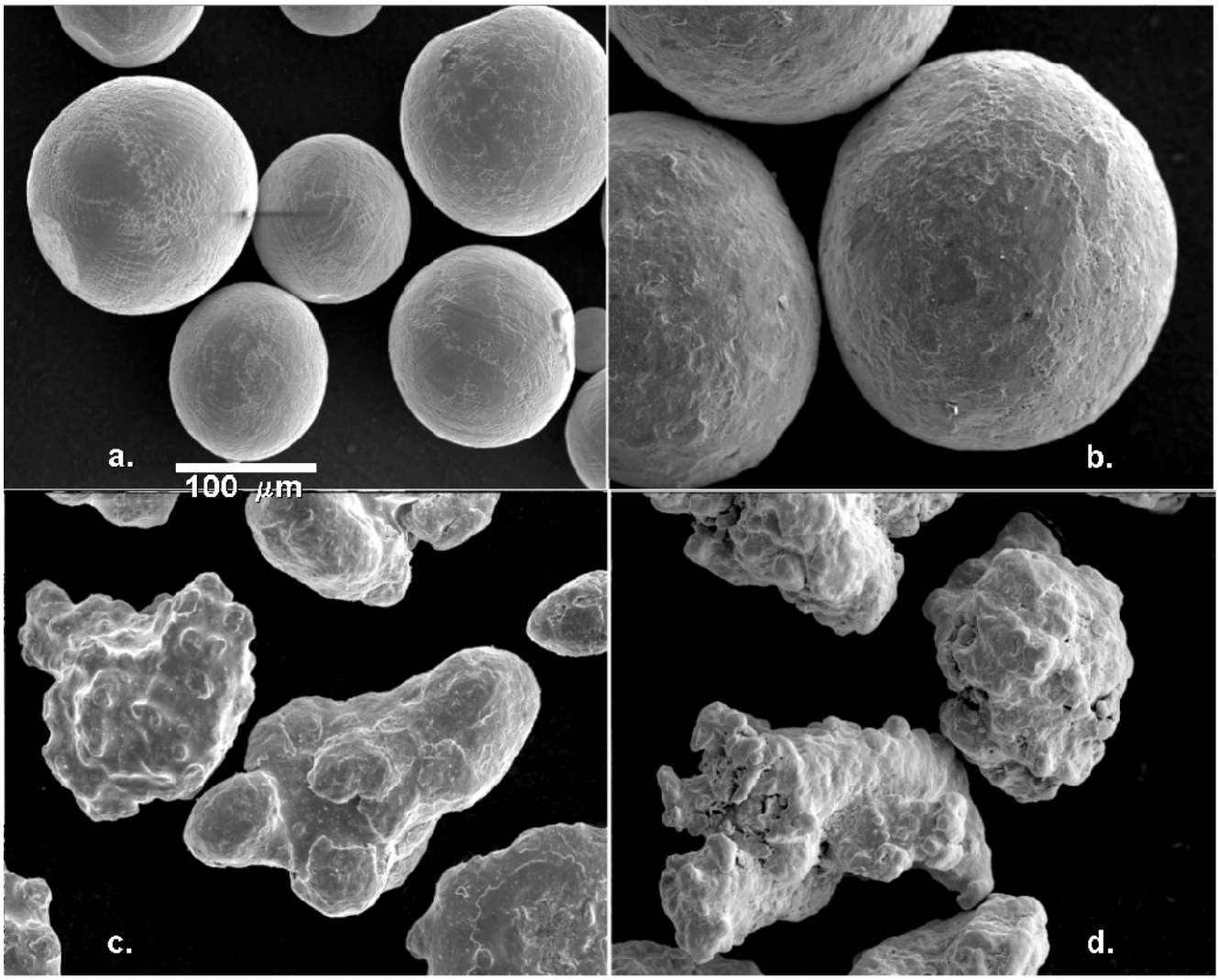

Figure 3. Scanning electron micrographs of four types of uncoated carrier particles: (a) smooth–round, (b) rough–round, (c) smooth–grit, (d) rough–grit.

of Eq. 3 to the data in Table II is 3.1 ± 0.3, with an index of determination of 0.98. This fit is not shown in Fig. 6; the curved line shown there is drawn through the data points.

Model for Dependence of Conductivity on Toner Concentration. Toner particles are much more insulating than the carrier beads. Consequently, if a toner particle rests in a junction between a pair of carrier beads, conduction is essentially cut off. We assume that the developer conductivity is given by the conductivity of the carrier beads times the probability of contact between them. The probability of contact depends on the toner concentration, which is related to the number of toner particles per carrier bead, n, by

$$C = \frac{n\rho_t r^3}{\rho_C R^3},$$

where ρ_t (ρ_C) is the mass density of the toner (carrier) and r (R) is the radius of the toner (carrier) . (Here C is expressed as a mass fraction; however, in the data analysis and plots, C will be expressed in parts per hundred, percent.)

Williamson, Greenwood, and Harris[8] have examined the influence of insulating dust particles on the electrical conductivity between a small gold needle with a hemispherical tip and a flat gold substrate. They showed that the probability of contact between the needle and a flat surface in the presence of n dust particles is given by

$$P_0 = \exp\left(-\frac{An}{S}\right), \quad (4)$$

where the area, A, is the region of influence of the dust particle in preventing a contact, and S is the area over which the dust particles are scattered. A key idea in the work of

TABLE II. Values of G_0 and B for a Developer with Various Toner Concentrations

Toner concentration (%)	Individual data sets		Combined data sets	
	G_0 (Ω^{-1})	B ($V^{-0.5}$)	G_0 (Ω^{-1})	B ($V^{-0.5}$)
0.16	6.3×10^{-7}	0.48	5.7×10^{-7}	—
0.55	2.2×10^{-7}	0.51	2.3×10^{-7}	—
1.30	4.8×10^{-8}	0.51	5.0×10^{-8}	—
1.55	1.3×10^{-8}	0.53	1.5×10^{-8}	—
1.97	3.0×10^{-9}	0.51	3.1×10^{-9}	—
2.32	5.6×10^{-10}	0.62	9.5×10^{-10}	—
2.77	2.0×10^{-10}	0.47	1.6×10^{-10}	—
All	—	—	—	0.50

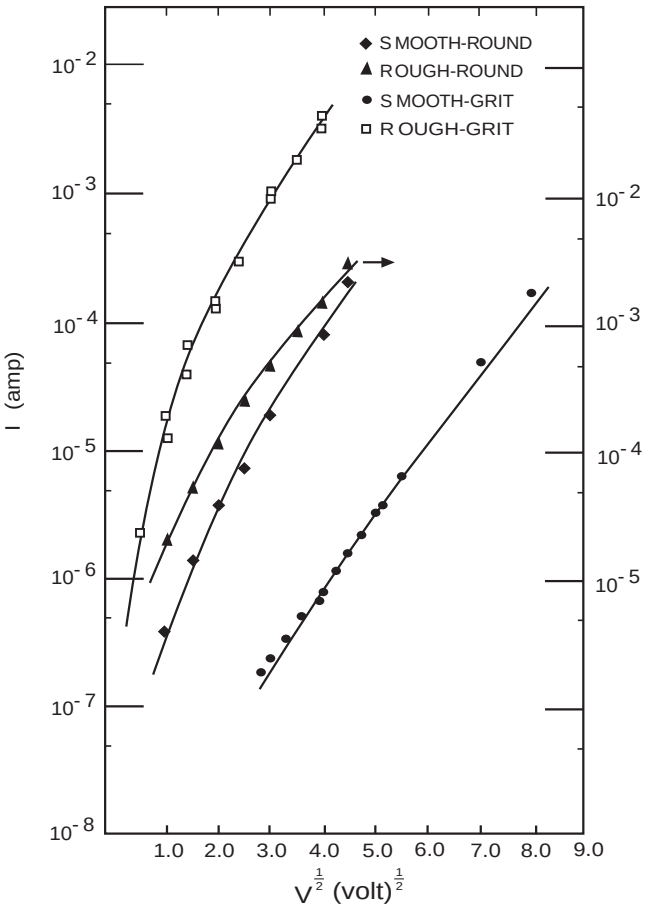

Figure 4. Current–voltage measurements of the four carrier materials shown in Fig. 3. The solid lines are calculated using Eq. 2 and the values of the parameters G_0 and B determined by a nonlinear least-squares method. The data for the rough–round carrier are referred to the right-hand scale.

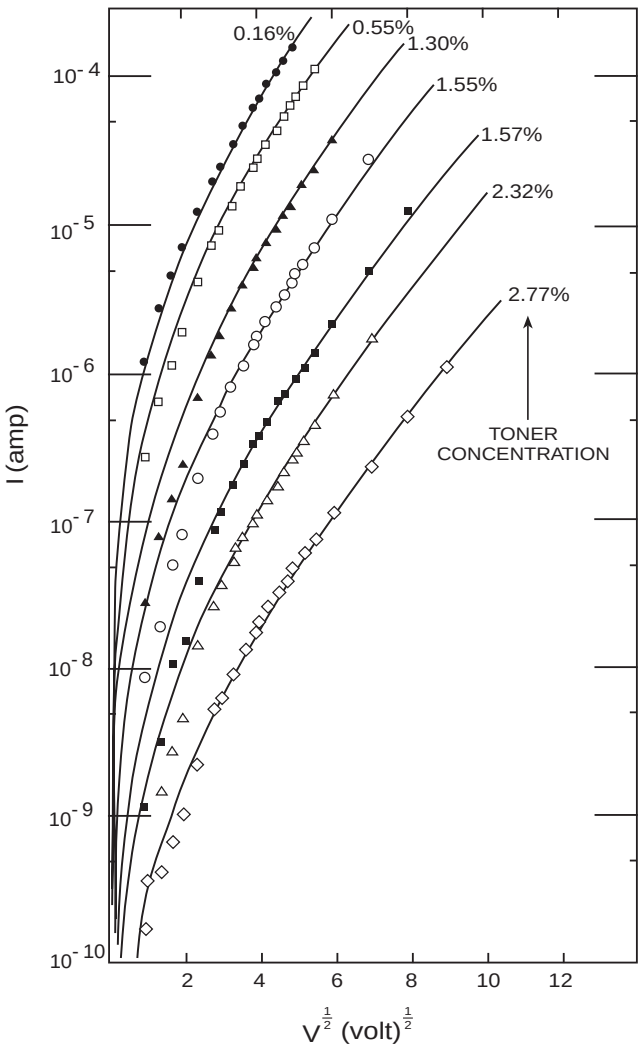

Figure 5. Current–voltage measurements of a developer material for different values of toner concentration. The solid lines were calculated using Eq. 2 with separate values of G_0 for each toner concentration and a common value of the parameter B.

Williamson, Greenwood, and Harris is that a dust particle need not be at the point of contact to prevent contact; but, it will prevent contact if it is anywhere within a certain distance from the point of contact. We will use this result to build a model for carrier beads covered with toner particles.

Smooth Spheres. The top of Fig. 7 illustrates two smooth, spherical carrier particles with radius, R, in contact with a toner particle of radius, r, positioned as close as possible to the point of contact without breaking it. The distance, x, of the toner particle from the axis defines the region of influence denoted by A, which is approximately $2\pi rR$. Analogous to the geometry of Williamson, Greenwood, and Harris, the probability of contact at a junction between a carrier bead covered with toner particles and one without any toner particles is, from Eq. 4, $P_0 = \exp(-\rho_C R^2 C/2\rho_t r^2)$, where we have used $S = 4\pi R^2$ for the area of the carrier bead. For the case of two adjacent carrier beads, each covered with toner particles, the joint probability of contact is the square of this probability, namely P_0^2.

The current flow in a 3-D developer layer depends on the arrangement of conducting junctions formed. This problem could be addressed using percolation models, but that approach will not be treated here. We propose two cases for current flow. In one case, the local electric field is assumed to be aligned with the direction of the applied field, and current flows only through the contacts in that direction. For this 1-D case, the joint probability of contact is P_0^2. In the other case, we assume that the local electric field is not aligned with the applied field, so that the local current does not necessarily flow in the direction of the applied field. Hence, for this case, we think of the developer as a 3-D network of unit cells having cubic symmetry. Each unit cell comprises a current-donating bead and three beads that could receive current. The maximum conductivity of the unit cell occurs when all three junctions conduct, which has a joint probability of contact of $(P_0^2)^3$. Alternatively, the smallest nonzero value of conductivity for the unit cell occurs when only one junction conducts, with probability P_0^2, similar to the probability for the 1-D case.

For the purpose of analysis of the developer conductivity data, we have selected $(P_0^2)^3$ to use in the model, because this term gives values of carrier radius inferred from the conductivity data that agree with the measured values. With this assumption, and using Eq. 4, the probability of contact is

$$P_s(C) = \exp(-\alpha_s C), \tag{5}$$

where

$$\alpha_s = \frac{3\rho_C R^2}{\rho_t r^2}.$$

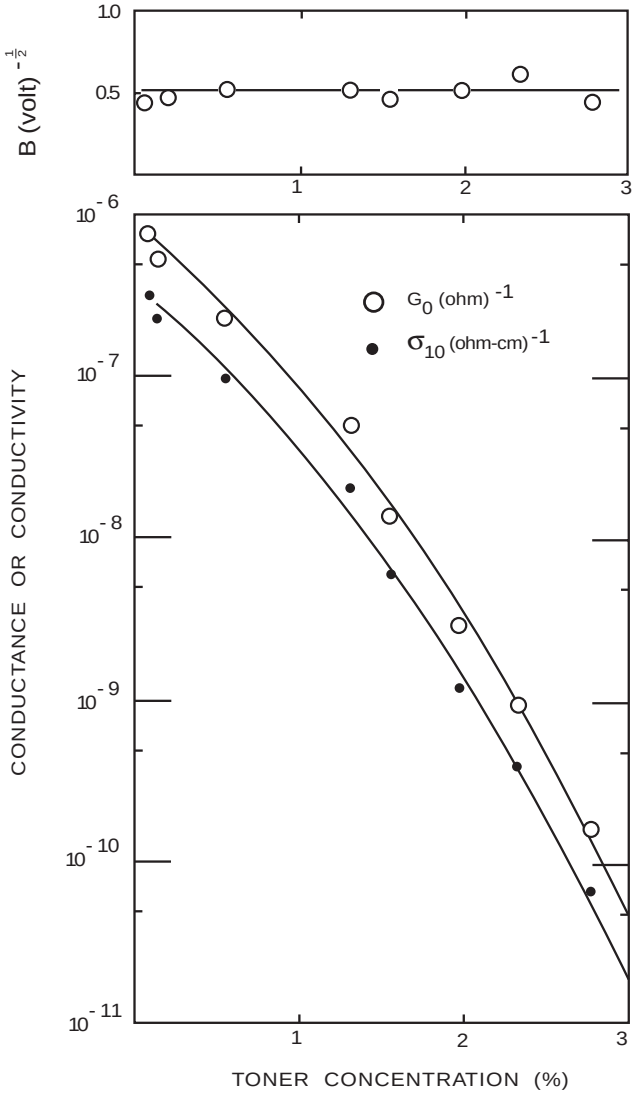

Figure 6. Values of the parameters G_0 and B from nonlinear least-squares fits of Eq. 2 to the data in Fig. 5. In this case, separate values of G_0 and B were determined for each toner concentration. The parameter B is independent of toner concentration, whereas the parameter G_0 is strongly dependent on toner concentration. Values of conductivity measured with a 10 V bias, σ_{10}, are shown for comparison.

Rough Spheres. If the carrier surfaces are rough, toner particles can sit in the "valleys" on the carrier surface without breaking the contact between two carrier beads; the bottom of Fig. 7 illustrates this geometry. We characterize the average depth of the valleys by the parameter δ. Because the toner particle can sit in the valley, the region of influence is reduced; the height of the toner particle is effectively reduced from r to $r - \delta$. This condition modifies A to $2\pi(r\text{-}\delta)R$, if $r > \delta$, and A is zero if $r < \delta$. By analogy to Eq. 5 we find

$$P_r(C) = \exp(-\alpha_r C), \tag{6}$$

where

$$\alpha_r = \begin{cases} \dfrac{3\rho_C(r-\delta)R^2}{\rho_t r^3}, & r > \delta \\ 0, & r \le \delta. \end{cases}$$

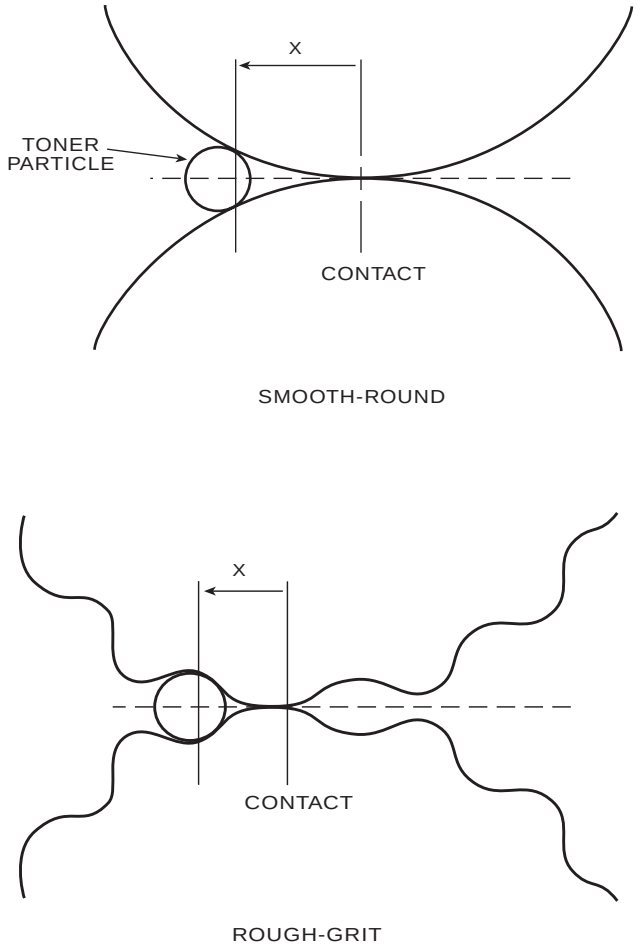

Figure 7. Geometry in the region of contact between two carrier beads about to be interrupted by an insulating toner particle. The two drawings are for smooth and rough carrier beads, respectively. The drawing shows that for the rough carrier beads, the region of influence (radius indicated by x) is reduced.

We note that α_r reduces to α_s when the carrier surface roughness is zero, so that we can drop the subscript notations r and s. Eqs. 5 and 6 apply to the 3-D network. (For the limiting case where the local current flows only in the direction of the applied field, α is one-third as large.) Using the assumption that the developer conductivity is given by the conductivity of the carrier beads, $G_0(0)$, multiplied by the probability of contact between them, we have

$$G_0(C) = G_0(0)P(C). \tag{7}$$

This expression for $G_0(C)$ is similar to the empirical relationship in Eq. 3. The physical model predicts a specific dependence of the parameter α on toner and carrier size and on carrier surface roughness that will be tested in the next section.

Dependence of α on Toner and Carrier Geometry. The toners used in these experiments were air classified into narrow size distributions, about 5 μm wide, characterized by the number median diameter. To obtain a measurement for very small particles, 1.0 μm diameter aluminum oxide was used. Four types of uncoated carriers shown in Fig. 3 were selected: smooth–round, rough–round, smooth–grit, and rough–grit particles. These samples have morphologies similar to that of the carriers used for the current–voltage data in Fig. 4, but they are from different lots with different oxide layers. Carrier diameters were determined by sieve analysis.

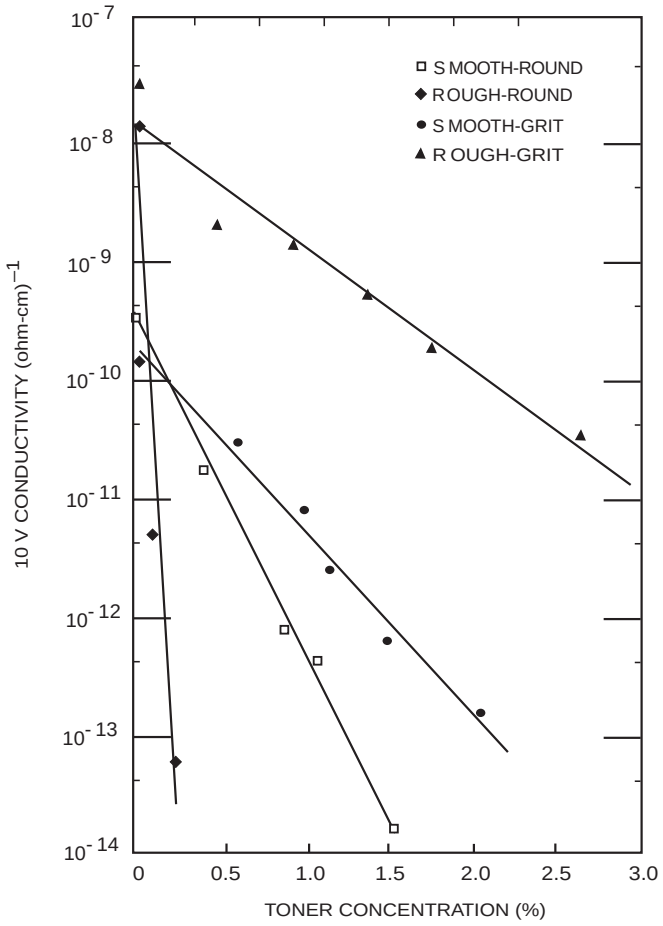

Figure 8. Example of the toner concentration dependence of the conductivity measured on developers made with the four types of carrier beads shown in Fig. 3, each mixed with 10-μm diameter toner particles.

Rather than measuring the entire I–V curve, a single conductivity measurement at 10 V, σ_{10}, was used for expediency because B was independent of toner concentration, as previously discussed. As shown in Fig. 6, a good correlation was confirmed between σ_{10} and the value of G_0 determined from the I–V data. An example of the dependence of σ_{10} on toner concentration is shown in Fig. 8 for the four types of carrier beads mixed with 10 μm diameter toner particles.

The semilogarithmic slope, α, was determined from the data by least-squares analysis. The values of α and $\mathcal{R}^2$, the index of determination, are listed in Table III. The dependence of α on toner size is shown in Fig. 9, where αd^3 is plotted against d, the number median toner diameter, as suggested by Eq. 6. A straight line is expected, having an intercept of 2δ and slope proportional to D^2, where D is the carrier diameter. The values of the carrier diameter and valley depth, δ, determined from the regression analysis, are listed in the lower section of Table III. The regression values of δ are consistent with optical microscopic observations of the surface texture of the carrier beads. The surface texture of the carrier beads was also characterized by using the topographic tracing capability of an atomic-force microscope (AFM). These measurements are shown in the lower section of Table III. There is very good agreement between the valley depth obtained from AFM topographic tracing and the valley depth calculated from the model. The AFM measurements on the rough-grit carrier also indicated deep valleys greater than 8 μm that we attribute to the shape of the beads. Because of our assumption that the conductivity is proportional to $(P_0^2)^3$, the agreement between the measured carrier diameters and those calculated from the model for α, Eq. 6, is good.

To investigate the dependence on carrier size more explicitly, additional measurements were made on a set of five carrier samples prepared by sieving a large quantity of a single sample of carrier. The toner used in these measurements had a broader size distribution than that of the previous set of toners. The results, which are plotted in Fig. 10, show that α increases proportionally as the square of the carrier diameter. The slope of this line is $(1.0 \pm 0.1) \times 10^{-4}$ μm^{-2} for C measured in percent. Our estimate for the slope based on the toner size is 1.2×10^{-4} μm^{-2}, which is in good agreement with the model.

Dependence of Developer Conductivity on the Frictional Properties of Toner and Carrier. The model described here assumes that the toner particles are "stuck" to the carrier beads so that the toners remain in place when the magnetic force pulls the carrier beads together. Williamson, Greenwood, and Harris,[8] whose experiments were referred to earlier, found that the dust particles sometimes moved when the gold tip was lowered onto them, which resulted in more numerous conducting contacts than expected from Eq. 4. When the dust particle was off the center of the tip but in position to prevent contact, a frictional force between the dust particle and the flat plate held the dust particle in place. Williamson, Greenwood, and Harris modeled the effect of slipping particles by adding to the probability of contact a term representing the fraction of particles, L, that should prevent contact but do not; this term is given by $L(1–P_0)$.

A similar situation occurs for two-component developers. Figure 11 illustrates the forces acting on a toner particle squeezed between two carrier beads. The mechanical and magnetic forces on the carrier beads act on the toner particle to push it out of the gap; this effect is counterbalanced by the friction force between the toner and carrier surfaces. If the toner particles can be pushed out of the gap, $P(C)$ in Eq. 7 underestimates the contact probability. Analogous to Williamson's treatment of slipping particles, the probability of contact in Eq. 7 should be modified to include two terms. The first term is for toner particles that stay in position, and the second term is for toner particles that should prevent contact but do not (because they are pushed aside). Thus it is plausible that the total probability of contact in Eq. 7 should be modified to

$$P(C) \rightarrow P(C) + L[1–P(C)], \tag{8}$$

where L is the fraction of the particles that should prevent contact but do not because they are pushed aside. The parameter L depends on the forces holding the toner particles in place; the larger the force, the smaller the value of L. As illustrated in Fig. 11, the tangential component of the magnetic force may be large enough to push the toner particle out of the region of influence, permitting the carrier beads to make contact. The toner particle will not move if this force is balanced by the frictional force. The normal force depends on the magnetic force and the electrostatic force, as indicated in Fig. 11.

We designed experiments to investigate these effects. The coefficient of friction can be varied by using toners with zinc stearate, which is a well-known cleaning blade lubricant. The electrostatic component of the force can be investigated by modifying the charge-to-mass ratio, q/m, of the toner particles with a charge control additive.

Electrostatic Force. We selected two toner samples having, respectively, a large and a small value of A_0, which

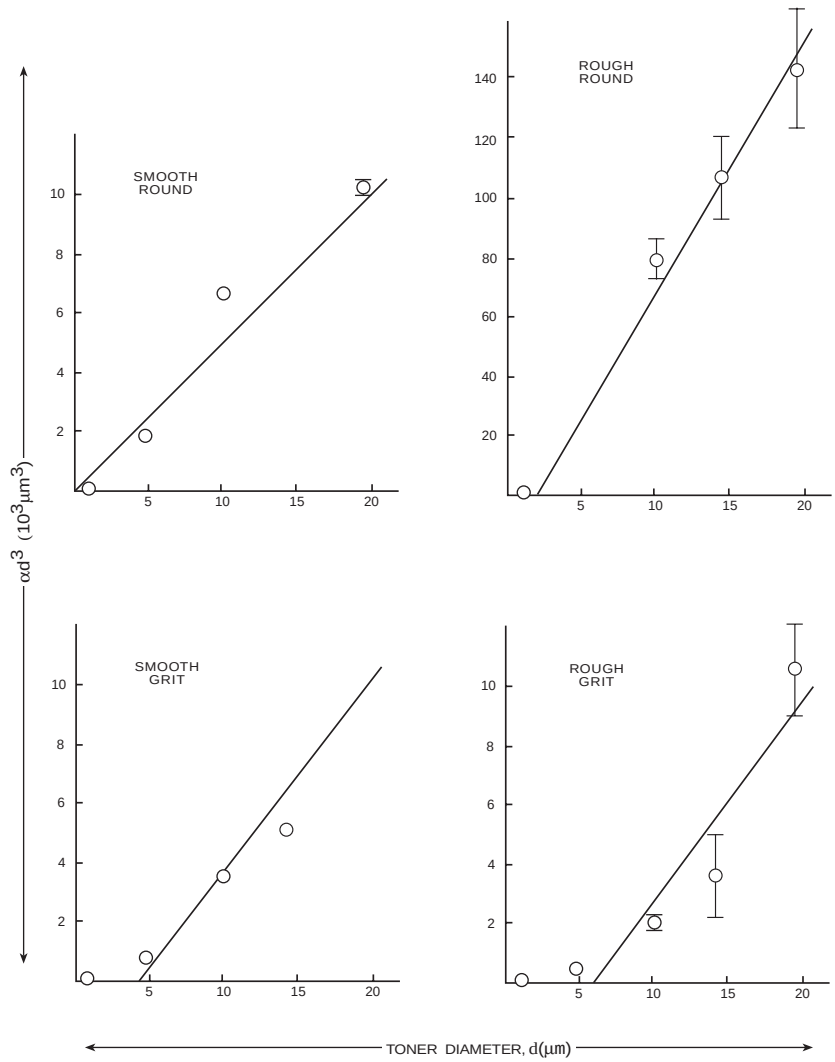

Figure 9. Values of the parameter αd^3 measured as a function of toner size for the four types of carrier beads shown in Fig. 3. The values of α were determined by a least-squares method using Eq. 7.

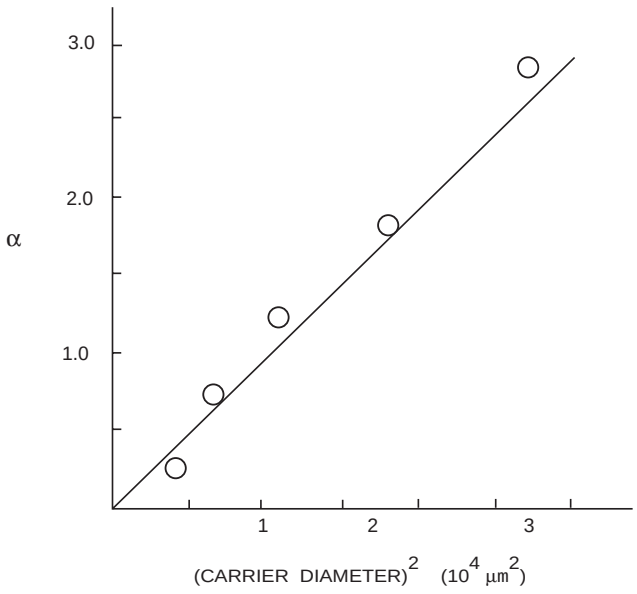

Figure 10. Measurements of the parameter α plotted as a function of the square of the carrier bead diameter. Eq. 6 predicts a proportional relationship and is in agreement with the measurements.

describes the triboelectric properties of the developer[9], to obtain large and small values of q/m for similar toner concentrations. Because we are examining primarily geometrical effects, it is not necessary to know the detailed toner composition. The toner size distributions were the same and the average size was 11 μm. The carrier was a rough–grit material with a diameter of 160 μm. Figure 12 shows the 10 V developer conductivity measurements as a function of toner concentration for developers made with each of the two toners. The lines are the result of a fit using two free parameters in Eq. 8. The term $P(C)$ is given by Eq. 6 with α as a free parameter. The parameter L is assumed to be proportional to the reciprocal of the force holding the toner particle in place. For the electrostatic image force of attraction between the toner particle and carrier bead, L is proportional to $(q/m)^{-2}$, with the proportionality constant a free parameter. The agreement between the measured and regression values shown in Fig. 13 suggests that the conductivity is increased when the electrostatic force between toner particle and carrier bead is small enough to allow toner particles to be pushed aside, out of the region of contact. Overall, the effect of the normal force is small for q/m values of interest in xerography and negligible for the measurements of α reported in Table III. Changes in the coefficient of friction have a much larger effect.

Coefficient of Friction. It is well known from investigations of blade cleaning that zinc stearate blended externally on toner particles can be used as a lubricant to reduce

TABLE III. Results of Measurements on Four Types of Carrier Beads

Morphology	Smooth–round		Rough–round		Smooth–grit		Rough–grit	
Values of α for different toner sizes								
Toner diameter (μm)	α	$\mathcal{R}^2$	α	$\mathcal{R}^2$	α	$\mathcal{R}^2$	α	$\mathcal{R}^2$
1.0*	27. ± 6.	0.95	N/M	—	3.91 ± 0.05	0.99	0	—
4.9	16.0 ± 0.3	0.99	99. ± 5.	0.99	6.1 ± 0.4	0.99	3.54 ± 0.14	0.99
10.1	6.4 ± 0.4	0.99	77. ± 6.	0.92	3.3 ± 0.2	0.98	1.9 ± 0.2	0.93
14.2	2.0 ± 0.1	0.98	37. ± 6.	0.92	1.76 ± 0.05	0.99	1.3 ± 0.5	0.61
19.3	1.42 ± 0.05	0.99	20. ± 3.	0.96	1.48 ± 0.13	0.97	1.5 ± 0.2	0.92
Values of carrier diameter and valley depth								
Diameter	D (μm)	$\mathcal{R}^2$	D (μm)	$\mathcal{R}^2$	D (μm)	$\mathcal{R}^2$	D(μm)	$\mathcal{R}^2$
Measured	96	—	263	—	93	—	95	—
Model	62 ± 5	0.92	255 ± 16	0.97	77 ±7	0.94	90 ±13	0.86
Valley depth	δ (μm)		δ (μm)		δ (μm)		δ (μm)	
Measured	0.25 ± 0.07	—	1.8 ± 0.6	—	2.0 ± 0.5	—	2.9 ± 0.2	—
Model	0.35 ± 1.0	0.92	1.3 ± 0.9	0.97	2.3 ± 1.2	0.94	3.0 ± 2.1	0.86
Carrier bead density								
Bulk density (g/cc)	4.5		4.5		3.7		3.1	

* Aluminum oxide particles (rather than toner particles) were used for the 1-μm measurements.

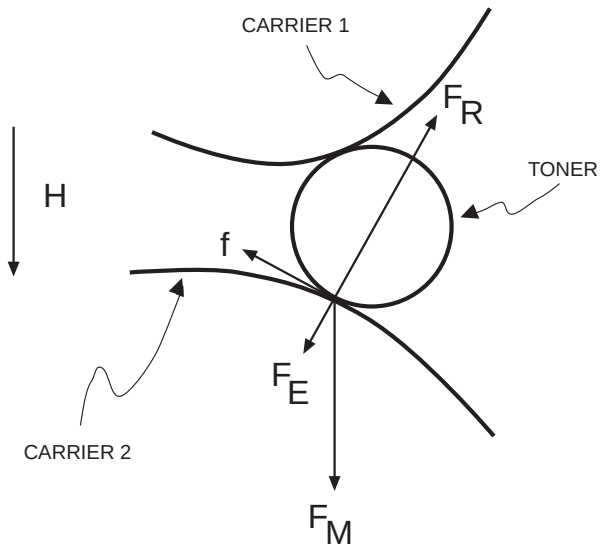

Figure 11. Diagram illustrating the forces at the point of contact between a toner particle and a carrier bead embedded in the developer. A similar force diagram applies to the other toner–carrier interface. The forces are the electrostatic force of attraction between carrier and toner F_E, the friction force at the toner–carrier interface f, the (normal) force of the carrier surface pushing against the toner particle F_R, and a force related to the magnetic forces acting on the carrier beads F_M.

the frictional force between a cleaning blade and the photoreceptor. We hypothesize that the same effect occurs between a toner particle and a carrier bead. Nash[10] has presented data for the effect of zinc stearate on developer conductivity. Figure 14 shows his developer conductivity data σ_{200} (measured using a 200 V bias) as a function of toner concentration for two developers, with and without zinc stearate on the toner. The zinc stearate has a large effect on the conductivity and its dependence on toner concentration. The physical model we propose is that toner particles with zinc stearate are able to slip out of the contact region, whereas toner particles without zinc stearate cannot slip out. Consequently, in Eq. 8, we assume that L has a constant value for developers with zinc stearate, and that L is zero for developers without. Figure 14 shows the result of fitting Eq. 8 to the data set using two values for L, a single value for α, and a single value for $\sigma_{200}(0)$ – the conductivity value at 0% toner concentration. The regression values are $\log_{10}\sigma_{200}(0) = -10.47$, $\alpha = 1.45$, and $L = 0.27$ or $L = 0$, for developers with and without zinc stearate, respectively. The agreement between the fitted model and measurements is excellent.

These two experiments demonstrate the plausibility of a physical model in which the toner particles can be pushed away from the region of contact in response to electrostatic and magnetic forces. The probability of movement depends on the coefficient of friction between the toner particle and the carrier bead and on the normal force between them.

Investigation of Dynamic Mode Conductivity

Carrier Beads. Up to this point, our investigation has focused on the static mode of measurement. When measurements are made in the dynamic mode, additional currents are generated. Figure 15 shows I–V data for a smooth–grit carrier coated with enough polymer to reduce the static conductivity by many orders of magnitude. There are three differences compared with the static mode data (an example was shown in Fig. 4). First, there is a large current with no voltage applied; second, the current does

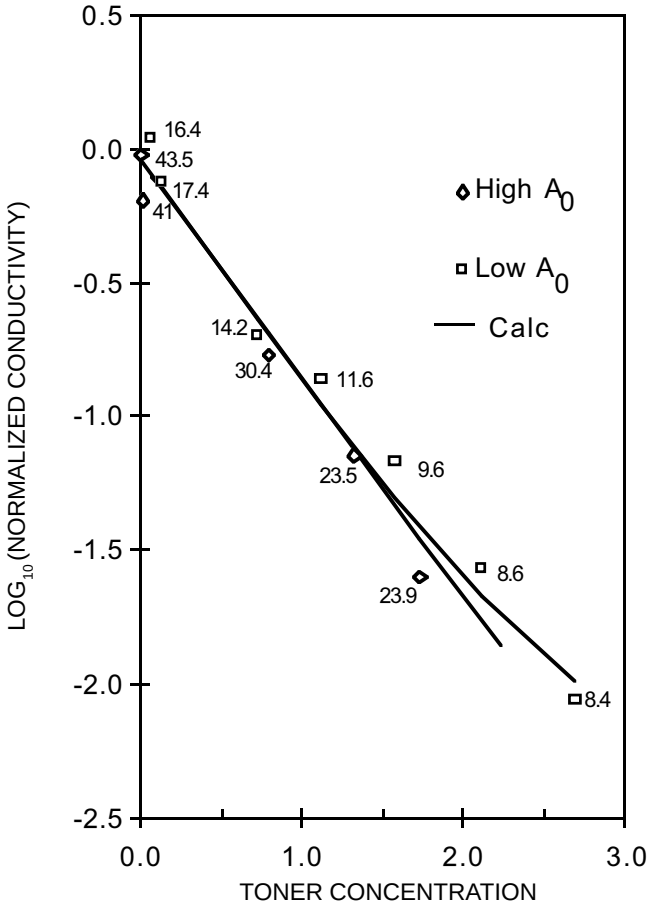

Figure 12. Measurements of conductivity as a function of toner concentration for two developers formulated with toners that give large and small values of the parameter A_0, respectively, leading to large and small values of q/m; the values are noted on the figure. The solid lines are calculated from Eqs. 6 and 8.

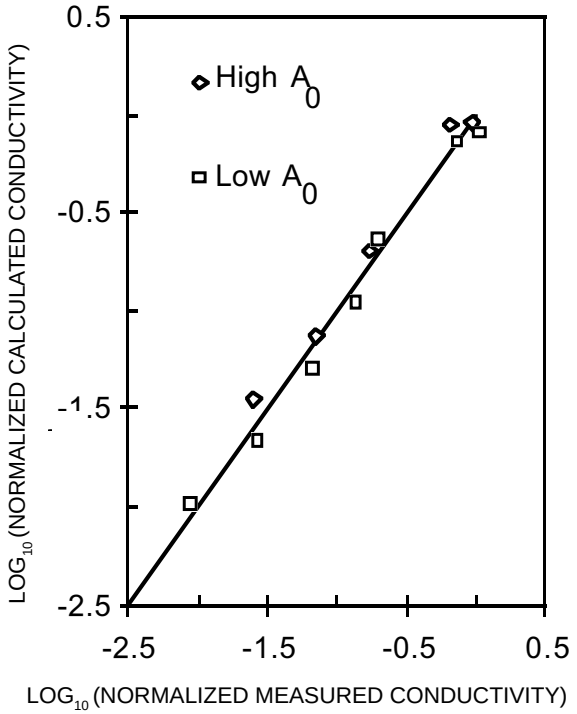

Figure 13. Comparison of the measured and fitted values of conductivity for the developers in Fig. 12.

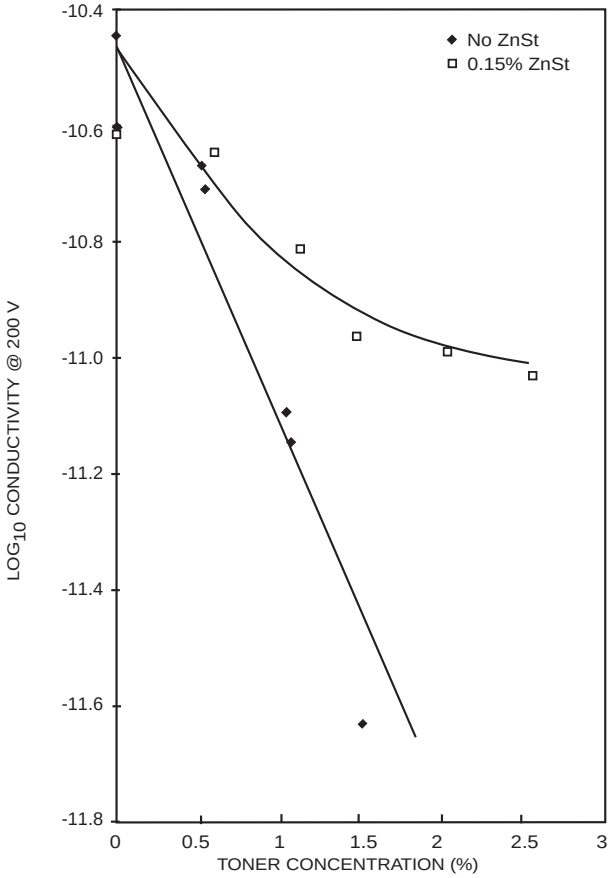

Figure 14. Measurements of conductivity as a function of toner concentration for developers using toners with and without zinc stearate (ZnSt). The solid lines are calculated from Eqs. 6 and 8, using parameter values determined by a least-squares fit to the data. The developer with zinc stearate is more conductive because the zinc stearate acts as a lubricant that enables toner particles to slide away from the region of contact.

not increase as rapidly with increasing voltage; and third, there is a "negative resistance" regime in which a positive current is measured even though the applied voltage is negative. Because of this behavior, the current–voltage data cannot be conveniently displayed on a semilogarithmic plot. The current with zero applied voltage depends on the type of polymer material used to coat the carrier. The carrier bead sample used in this experiment was designed to enhance the current at zero volts by choosing a polymer that has a different position in the triboelectric series from the aluminum electrode. The carrier rubbing against the guarded electrode introduces a triboelectric current in addition to the conduction currents. The triboelectric current is caused by contact charging between the carrier beads and the electrode surface, and it depends on the relative speed of the carrier beads and electrode. The contact charge, and therefore the triboelectric current, has both electric-field-independent and dependent components.[11]

The measured dynamic current is the sum of the conductive current and the triboelectric current. The triboelectric current also has two contributions, one independent of applied voltage and the other linearly dependent on the applied voltage. Consequently, the measured current can be written as

$$I_{meas} = I_{cond}(V) + I_{tribo}(V), \tag{9a}$$

with

$$I_{cond}(V) = \mathcal{G}_0 V \exp(B_D |V|^{0.5}), \tag{9b}$$

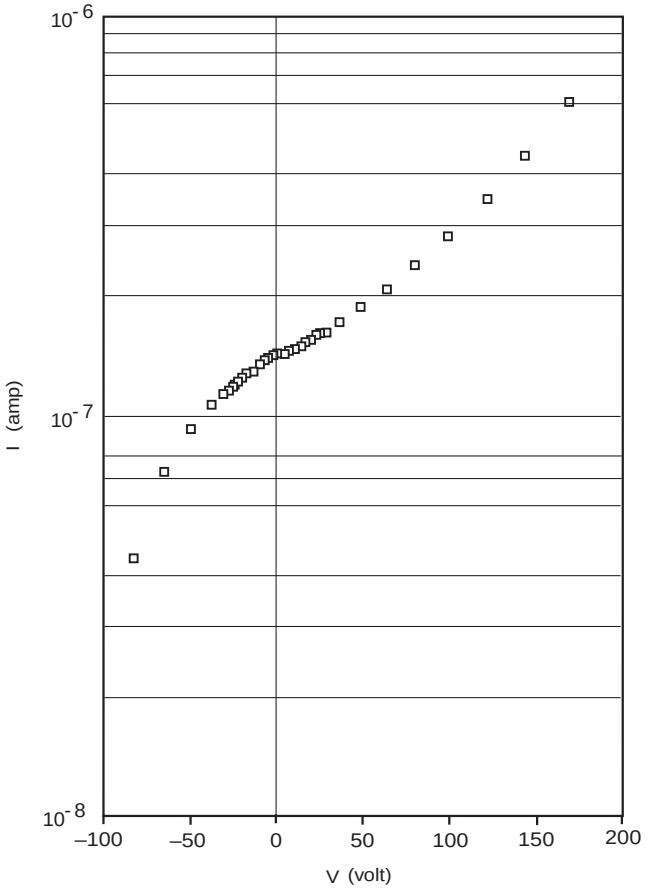

Figure 15. Current–voltage measurements made in the dynamic mode for a carrier sample. For zero applied voltage, there is a current generated by the triboelectric charging of the carrier rubbing against the electrode.

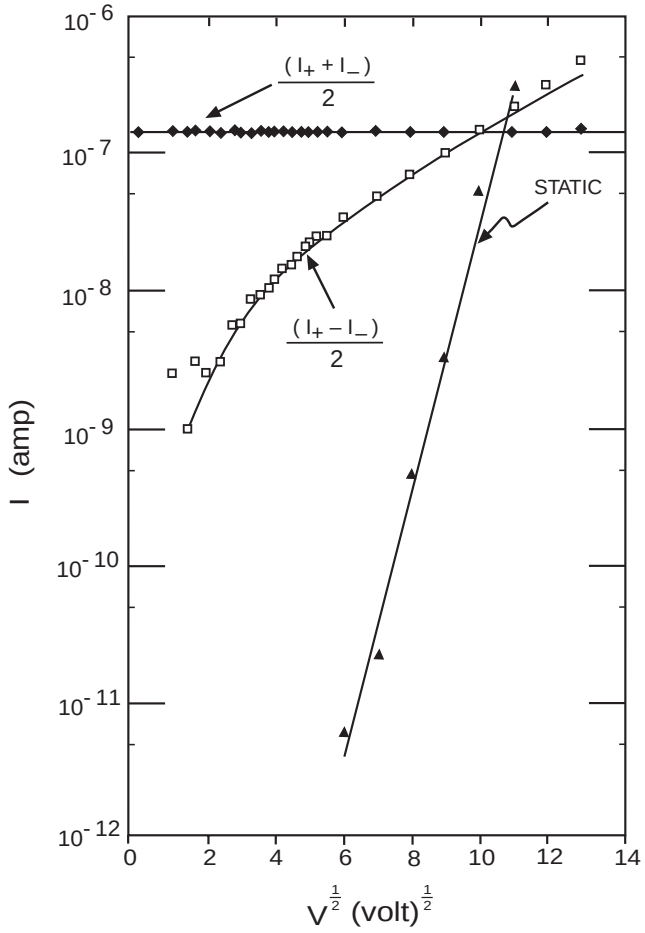

Figure 16. Dependence on applied voltage of the sum and difference of the currents measured with positive and negative applied voltage. The sum is independent of voltage; the difference depends strongly on voltage. Static mode measurements are shown for comparison. The lines for the dynamic mode results are regressions to Eq. 10.

and

$$I_{tribo}(V) = I_{0\ tribo} + \beta_T V, \tag{9c}$$

where $\mathcal{G}_0$ is the conductance in the dynamic mode, B_D is the value of B for the dynamic mode, $I_{0\ tribo}$ is the current with no applied voltage, and β_T is the coefficient of the electric-field-dependent triboelectric current.

We were able to separate the triboelectric and conductive components by measuring the total current for both positive and negative applied voltages. Then, by taking one-half the sum of the currents measured with positive and negative applied voltages, we obtained a current that is represented by an even function of the voltage; similarly, by taking one-half the difference of the currents for the positive and negative applied voltages, we obtained the current that is represented by an odd function of the voltage. The sum and difference currents are shown in Fig. 16. The sum is independent of the applied voltage whereas the difference is a rapidly increasing function of voltage. From Eq. 9, we find

$$I_{sum} = \frac{I_{meas}(+V) + I_{meas}(-V)}{2} = I_{0\,tribo} \tag{10a}$$

$$I_{diff} = \frac{I_{meas}(+V) - I_{meas}(-V)}{2} = \mathcal{G}_0 V \exp(B_D|V|^{0.5}) + \beta_T V. \tag{10b}$$

The constant current is due to the electric-field-independent component of the triboelectric current, $I_{0\,tribo}$. The average value is indicated by a solid line in Fig. 16. The difference current increases rapidly with voltage. This current is the sum of the Poole–Frenkel current and the field-dependent component of the triboelectric current, both of which are odd functions of the applied voltage. The line in Fig. 16 through these data is the parametric fit using Eq. 10(b). For comparison, the static I–V characteristic for this carrier is also shown in Fig. 16.

As shown in Table IV, the dynamic mode values of $\mathcal{G}_0$ and B_D are larger and smaller, respectively, than the corresponding values measured in the static mode. In the dynamic mode, the carrier beads are constantly forming and breaking contacts, which might degrade the quality of the contacts, mimicking a thicker oxide layer and resulting in a smaller value of the Poole–Frenkel coefficient B. We suspect that the large value of $\mathcal{G}_0$ is due to the displacement current caused by convective motion of charged beads toward the electrode. The bead charge, in turn, is enhanced by the Poole–Frenkel mechanism that is controlling current flow between beads.

Developers. In contrast to the static mode, in the dynamic mode of measurement toner can move toward the electrode or toward the rotating cylinder, depending on the polarity of the voltage. The motion of the charged toner

TABLE IV. Comparison of Dynamic and Static Mode Parameters

Parameter	Dynamic mode		Static mode	
Poole–Frenkel coefficient ($V^{-0.5}$)	B_D	0.16	B	2.0
Ohmic conductance (Ω^{-1})	$\mathcal{G}_0$	2.9×10^{-10}	G_0	6.7×10^{-19}
Field-independent tribo current (amp)	$I_{0\,tribo}$	1.4×10^{-7}	—	—
Field-dependent tribo coefficient (Ω^{-1})	β_T	1.6×10^{-10}	—	—

particles is detected as a current, so that Eq. 9 has an additional term and is modified to

$$I_{meas} = I_{cond}(V) + I_{tribo}(V) + I_{toner}(V). \tag{11}$$

We have found that I_{toner} depends on the polarity of the voltage; this is because the dynamics of deposition and scavenging are different for the two polarities.[1] For toner deposition on the electrode, the magnetic brush deposits and scavenges toner from the electrode, whereas for toner deposition on the cylinder, the magnetic brush deposits but does not scavenge toner from the cylinder surface because there is no relative motion between the developer and the rough cylinder. Consequently, the magnitude of I_{toner} measured for positive and negative voltages will be different:

$$\left|I_{toner}(+V)\right| \neq \left|I_{toner}(-V)\right|.$$

Because we do not know the voltage dependence of the toner migration current, we are not able to separate the measured current into individual currents by taking the sum and difference of the measured currents for the two polarities. However, we can examine the slope of the I–V data at zero volts, which we define to be the apparent dynamic conductance. If the polarity of the applied voltage is such that toner moves toward the rotating cylinder surface ("reverse bias"), the toner migration current will tend toward zero after several revolutions of the cylinder past the electrode. In the reverse bias case, toner accumulates on the cylinder surface because there is no relative motion between the developer beads and the surface, hence no scavenging of the toner particles. The amount of deposited toner accumulating on the cylinder surface is limited by the electric field of the toner charge. When the magnitudes of the toner electric field and the applied field are equal (the "neutralization limit"), the deposition stops and the toner migration current vanishes. For small values of the applied voltage, the amount of toner deposited on the cylinder surface is small and resides primarily in the "valleys" of the rough surface. Thus the cylinder will have good electrical contact with the developer. Consequently, in the reverse bias case, the toner current vanishes and the measured current from Eq. 11 is

$$\underset{reverse}{I_{meas}} \rightarrow I_{cond}(V) + I_{tribo}(V).$$

From Eqs. 11, 9(b), and 9(c), the apparent dynamic conductance in the reverse bias case is

$$\underset{reverse}{\mathcal{G}_{apparent}} = \left.\frac{dI}{dV}\right|_{\substack{0 \\ reverse}} = \mathcal{G}_0 + \beta_T.$$

Thus the apparent dynamic conductance is larger than the static conductance, which from Eq. 2 is G_0. With toner particles present, the dynamic conductance, $\mathcal{G}_0(C)$, is given by $\mathcal{G}_0(0)\exp(-\alpha C)$, the analog of Eq. 3. We expect the value of α to be the same for the dynamic and static modes because the toner–carrier geometry is unchanged. This is tested in Fig. 17, which compares the apparent dynamic conductivity, measured by the slope of the I–V data at zero volts, with the static conductivity, measured in a similar fashion. Both were measured at different toner concentrations, using a rough-grit carrier coated with a low weight of a polymer to reduce the triboelectric currents, so that β_T is small. For small values of the toner concentration, there is good agreement between the slopes measured in the two modes, indicating the same value of α. For larger values of toner concentration, the apparent dynamic conductance is dominated by the triboelectric current.

Discussion

We have made measurements of developer conductivity using a cell that replicates the magnetic field configuration and roll geometry in the xerographic development zone. The measurements were performed in two modes, static and dynamic. The static measurements, made with the roller at rest, reveal the conductive property of developer materials but do not replicate all of the currents that occur in xerographic development, particularly currents generated by triboelectric charge exchange between the developer and the photoreceptor and by toner migration. We developed a physical model for the static mode conduction current based on an investigation of the I–V characteristics of the carrier beads and the developer materials. We found that the static mode developer conductivity could be modeled by separating two phenomena. The first phenomenon is the current–voltage relation described by a Poole–Frenkel model for conduction through an oxide layer. The second phenomenon describes the probability that toner particles break the contact between two adjacent carrier beads. This probability depends on the toner concentration and on the geometrical properties of the toner particle and carrier beads.

A physical model for the dependence of static mode conductivity on toner concentration and on the geometrical

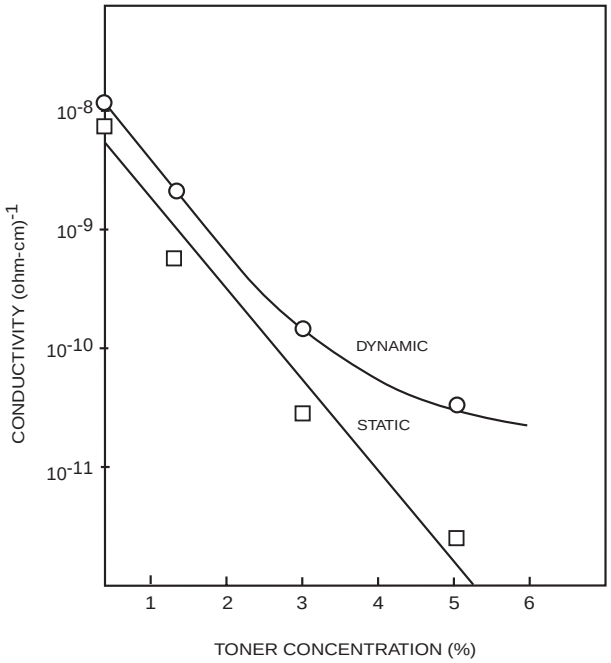

Figure 17. Comparison of dynamic and static mode conductance measurements for a rough–grit carrier. For small toner concentrations, the slopes are the same. For larger toner concentrations, the additional dynamic mode currents are much larger than the conductive current. The static mode measures only the conductive current at all toner concentrations.

properties of the carrier beads and toner particles was derived by examining the geometry of contact of two carrier beads covered with toner. The current–voltage relationship for static mode measurements is described by

$$I = G_0(0)\exp(-\alpha C)V\exp(BV^{0.5})$$

$$\alpha = \begin{cases} \dfrac{3\rho_C(r-\delta)R^2}{\rho_\tau r^3}, & r > \delta \\ 0, & r \le \delta. \end{cases} \tag{12}$$

This model assumed that the toner particles were not able to move on the surface of the carrier. However, we found that if a lubricant was added to the developer, the measured conductivity was higher than predicted by Eq. 12. We presented additional experiments that show the plausibility of a physical model in which the toner particles can be pushed away from the region of contact between two carrier beads in response to external forces that squeeze carrier beads together. The probability of movement depends on the coefficient of friction between the toner particle and carrier bead and on the normal force between them. The normal force has both electrostatic and magnetic components.

Relative to previous papers, our work extends Hoshino's investigation[4] by examining in more detail the dependence of developer conductivity on toner concentration and deriving a corresponding physical model. Hays[2] has also investigated the conductive properties of two-component developers. Hays' cell, which has a dielectric layer with properties similar to those of a photoreceptor, represents some aspects of the development zone more faithfully and thus is useful for modeling the development physics. The measurement cell and technique used by Hays are sufficiently different from ours that it is difficult to test our model, Eq. 12, using his data. Both sets of measurements on carrier beads indicate a strong electric field dependence of the current. However, his measurements of induced charge for developers show a weaker dependence on toner concentration than do our I–V measurements. Although this result seems to imply a much smaller value of α, the interpretation of the induced charge measurement is not easily related to the I–V measurements that we used to determine α. There are two considerations. First, we would have to do an analysis to relate the charge accumulated during a voltage pulse on the dielectric material in his cell to our I–V measurement, because of the interaction between the electric-field-dependent conductivity and the accumulating charge. Second, the developer agitation and the external forces on the samples are different. The external force, as others[12] have shown, affects the quality of electrical contacts between metal beads. Our cell was designed to agitate the sample aggressively as it is transported by the roller. The sample is then compressed by the roller and electrode as the sample enters the measurement zone. Hays' cell, particularly with lower values of the magnetic field, produces a weaker force, and we speculate that this force affects the quality of bead-to-bead electrical contacts, modifying the I–V curve and the induced charge measurement. Hoshino[4] found that the I–V properties of a developer depended on the magnetic field; it is plausible that some of this effect was due to the change in the quality of the bead-to-bead contacts as the magnetic field was varied.

In the dynamic mode of measurement, there are three additional current contributions. The first is generated by contact electrification between the moving developer brush and the measurement electrode. The second is generated by the migration of charged toner through the brush. The third is a displacement current generated by the convective motion of the charged carrier beads, where the bead charge is enhanced by the Poole–Frenkel mechanism. These currents are included in Eq. 11. We presented measurements on carrier and developer materials that illustrate the relative magnitudes of the contributions of each of these currents. Additional work is required to develop a more complete physical model for dynamic-mode current measurements.

Inspection of the data in Fig. 6 shows that the conductivity decreases exponentially at low toner concentrations and then decreases even more rapidly at higher concentrations. This result is evidence of a percolation mechanism for conductivity in the developer sample. A model for developer conductivity based on percolation theory is a subject for future work.

Acknowledgments. We thank D. Juda, J. Mammino, and K. Stamp for materials and measurements, S. Kittelberger for the measurements in Fig. 10, and M. Ott for the AFM topographic measurements listed in Table III. We also thank C. Gage for discussions on the correspondence between the conductivity measurement and the magnetic force shown in Fig. 2, and we thank J. Laing for discussions about dynamic mode currents. Finally, we thank an anonymous reviewer for comments that helped us clarify several critical points.

References

1. J. Benda and W. J. Wnek, A model for magnetic brush development in xerographic machines, *IEEE Trans. Industry Appl.* **IA-17**: 610 (1981).
2. D. A. Hays, Electrical properties of conductive two-component xerographic developer, *IEEE Trans. Industry Appl.* **IA-23**: 970 (1987).
3. J. J. Folkins, Intermediate conductivity—The crossover function for insulative and conductive two-component magnetic brush development in electrophotography, *IEEE Trans. Industry Appl.* **IA-24**: 250 (1988).
4. Y. Hoshino, Conductivity mechanism in magnetic brush developer, *Jap. J. Appl. Physics* **19**: 2413 (1980).
5. R. J. Nash and J. T. Bickmore, Toner impaction and conductivity aging, *Eighth International Congress on Advances in Non-Impact Printing Technologies*, 1992, p.131.
6. (a) J. G. Simmons, Electronic conduction through thin insulating films, *Handbook of Thin Film Technology*, L. I. Maissel and R. Glang, Eds., 1970, p. 1-14; (b) *Phys. Rev. Letters* **15**: 967 (1965).
7. Handbook of Chemistry and Physics, David R. Lide, Ed., CRC Press, Boca Raton, 1996, p. 12-47.
8. J. B. P. Williamson, J. A. Greenwood, and J. Harris, Influence of dust particles on the contact of solids, *Proc. Royal Society* **A237**: 560 (1956).
9. (a) E. J. Gutman and G. C. Hartmann, Triboelectric properties of two-component developers for xerography," *J. Imaging Sci. Technol.* **36**: 335 (1992); (b) The role of the electric field in triboelectric charging of two-component xerographic developers, *ibid* **39**: 285 (1995).
10. R. J. Nash, The effect of external additives on the conductivity of ferrite-based xerographic developers," *IS&T's Fifth International Congress on Advances in Non-Impact Printing Technologies*, 1989, p. 158.
11. D. A. Hays, Contact electrification between mercury and polyethylene: effect of surface oxidation, *J. Chem. Physics* **61**: 1455 (1974).
12. H. Ottavi, J. Clerc, G. Giraud, J. Roussenq, E. Guyon, and C. D. Mitescu, Electrical conductivity of a mixture of conducting and insulating spheres; An application of some percolation concepts, *J. Phys. C: Solid State Phys.* **11**: 1311 (1978).